Constraining nonstandard neutrino interactions with electrons

D. V. Forero[1,2,*] and M. M. Guzzo[2,†]

[1]*AHEP Group, Instituto de Física Corpuscular - CSIC/Universitat de València,*
Edificio Institutos de Paterna, Apt 22085, E-46071 Valencia, Spain
[2]*Instituto de Física "Gleb Wataghin" Universidade Estadual de Campinas,*
UNICAMP Rua Sérgio Buarque de Holanda, 777 13083-859 Campinas, São Paulo, Brasil
(Received 27 October 2010; revised manuscript received 1 April 2011; published 5 July 2011)

We update the phenomenological constraints of the nonstandard neutrino interactions (NSNI) with electrons including in the analysis, for the first time, data from LAMPF, Krasnoyarsk, and the latest Texono observations. We assume that NSNI modify the cross section of elastic scattering of (anti) neutrinos off electrons, using reactor and accelerator data, and the cross section of the electron-positron annihilation, using the four LEP experiments, in particular, new data from DELPHI. We find more restrictive allowed regions for the NSNI parameters: $-0.11 < \varepsilon_{ee}^{eR} < 0.05$ and $-0.02 < \varepsilon_{ee}^{eL} < 0.09$ (90% C.L.). We also recalculate the parameters of tauonic flavor obtaining $-0.35 < \varepsilon_{\tau\tau}^{eR} < 0.50$ and $-0.51 < \varepsilon_{\tau\tau}^{eL} < 0.34$ (90% C.L.). Although more severe than the limits already present in the literature, our results indicate that NSNI are allowed by the present data as a subleading effect, and the standard electroweak model continues consistent with the experimental panorama at 90% C.L. Further improvement on this picture will deserve a lot of engagement of upcoming experiments.

I. INTRODUCTION

Observations of neutrinos coming from the Sun, from nuclear reactors, from cosmic ray collisions in the high atmospheric altitudes and neutrinos observed in accelerator beams offer compelling evidence in favor of the neutrino oscillation hypothesis (for a complete panorama of this subject, see [1] and references therein). The oscillation phenomenon requires an extension of the minimal version of the electroweak sector of the standard model (SM) [2] including lepton mixing and neutrino masses. In general, SM extensions, beyond providing neutrino masses and mixing, also generate new interactions. These are the so-called nonstandard neutrino interactions (NSNI).

In an model independent way, NSNI could arise, establishing the SM gauge principle at energies near the electroweak breaking, including new nonstandard bosons [3,4]. Whatever the origin of the new interactions, it is important to quantify its strength. New interactions have to be included without spoiling neutrino oscillations and several other SM predictions which are consistent with the present experimental picture. In particular, NSNI strength can be estimated from neutrino phenomenology.

The effective Lagrangian which parametrizes the NSNI is given by [5–8]:

$$- \mathcal{L}_{\text{eff}}^{\text{NSNI}} = \varepsilon_{\alpha\beta}^{fP} 2\sqrt{2} G_{\text{F}} (\bar{\nu}_\beta \gamma^\rho L \nu_\alpha)(\bar{f} \gamma_\rho P f), \quad (1)$$

where G_{F} is the Fermi constant, α and β represent the leptonic flavor, f refers to the fermions of the first family ($f = e, u, d$), and P represents the chiral operators ($P = R, L$).

The NSNI strength is taken into consideration in the $\varepsilon_{\alpha\beta}^{fP}$ parameters. The NSNI could conserve the lepton flavor, in which case it is called flavor diagonal (FD) $\alpha = \beta$, or not, when it is called flavor changing $\alpha \neq \beta$.

In this work, we address the sensitivity of the present data on constraining the NSNI with electrons ($f = e$). We use LSND, Irvine, Rovno, and MUNU experimental data which have already been used to constrain NSNI [6] adding, for the first time in this kind of analysis, LAMPF [9], Krasnoyarsk [10] and, in particular, the latest Texono data [11] to find limits on FD parameters ε_{ee}^{eP} ($P = R, L$). Also, we consider the cross section for the process $e^+ e^- \rightarrow \nu \bar{\nu} \gamma$ measured in the LEP experiments: ALEPH, OPAL, and L3 (elsewhere in Refs. [8,12]) including new data from the DELPHI experiment [13] to constrain $\varepsilon_{\alpha\alpha}^{eP}$ ($P = R, L$) with $\alpha = e, \tau$.

Our analysis constrains NSNI in more stringent ranges than the ones found in the literature. These results indicate that NSNI are allowed by the present data as a subleading effect and the standard electroweak model continues, consistent with the experimental at 90% C.L.

The present article is organized as follows: to constrain the FD NSNI $\varepsilon_{\alpha\alpha}^{eP}$ ($\alpha = e, \tau$) parameters, first, we will use neutrino elastic scattering cross section data in Sec. II. Second, we will calculate the NSNI constrains from the cross section for process $e^+ e^- \rightarrow \nu \bar{\nu} \gamma$ using the four LEP experiments, in Sec. III. Then, we perform the global analysis for the ε_{ee}^{eP} parameters in Sec. IV. The summary and conclusion are presented in Sec. V.

II. NEUTRINO ELASTIC SCATTERING

For low energies, the neutrino-electron elastic scattering can be described by a SM effective theory [5]:

---

*dvanegas@ific.uv.es
†guzzo@ifi.unicamp.br

TABLE I. Experiments added with respect to Ref. [6], in order to constrain the NSNI parameters ε_{ee}^{eP}.

Experiment	T [MeV]	Cross Section
LAMPF $\nu_e e$	7–60	$\sigma = [10.0 \pm 1.8]E_\nu \times 10^{-45}$ cm^2 [9]
Krasnoyarsk $\bar{\nu}_e e$	3.15–5.175	$\sigma = [4.5 \pm 2.4] \times 10^{-46}$ cm^2 fis^{-1} [10]
Texono $\bar{\nu}_e e$	3–8	$R = [1.08 \pm 0.26] \times R^{SM}$ [11]

$$-\mathcal{L}_{\text{eff}} = 2\sqrt{2}G_{\text{F}}\{(\bar{\nu}_e\gamma^\mu L\nu_e)(\bar{e}\gamma_\mu Le) + (\bar{\nu}_\alpha\gamma^\mu L\nu_\alpha)(g_R^e\bar{e}\gamma_\mu \text{Re} + g_L^e\bar{e}\gamma_\mu Le)\}, \quad (2)$$

with $\alpha = e, \mu, \tau$. The SM couplings with the Z boson are $g_R^e = \sin^2\theta_W$ and $g_L^e = -1/2 + \sin^2\theta_W$.

For neutrino interactions with electrons $f = e$, the NSNI Lagrangian in Eq. (1) takes a form that looks like the SM one in Eq. (2) with the SM couplings replaced by the new parameters ε_{ee}^{eP}, in the form:

$$-\mathcal{L}_{\text{eff}}^{\text{NSNI}} = 2\sqrt{2}G_{\text{F}}\{(\bar{\nu}_e\gamma^\mu L\nu_e)(\bar{e}\gamma_\mu Le) + (\bar{\nu}_\alpha\gamma^\mu L\nu_\alpha) \\ \times (\varepsilon_{ee}^{eR}\bar{e}\gamma_\mu \text{Re} + \varepsilon_{ee}^{eL}\bar{e}\gamma_\mu \text{Le})\}. \quad (3)$$

Adding the effective SM theory in Eq. (2) to the NSNI Lagrangian in Eq. (3) for $f = e$, we see the NSNI effect is the rescaling of the couplings in the form $g_P^e \rightarrow g_P^e + \varepsilon_{ee}^{eP}$.

Now, it is simple to include the modifications to the SM cross section from the new interactions.

A. Cross section

The differential elastic scattering cross section for the process $\nu_e e \rightarrow \nu_e e$ including the NSNI is [6]

$$\frac{d\sigma(E_\nu, T)}{dT} = \frac{2G_{\text{F}}^2 m_e}{\pi}\left[\bar{g}_L^2 + \bar{g}_R^2\left(1 - \frac{T}{E_\nu}\right)^2 - \bar{g}_L\bar{g}_R\frac{m_e T}{E_\nu^2}\right], \quad (4)$$

where G_{F} is the Fermi constant, E_ν is the neutrino energy, T is the electron recoil energy, and m_e its mass. As we argued before, the SM couplings are rescaled, and we defined the new couplings as

$$\bar{g}_R \equiv g_R^e + \varepsilon_{ee}^{eR}, \qquad \bar{g}_L \equiv 1 + g_L^e + \varepsilon_{ee}^{eL}. \quad (5)$$

To include the antineutrino elastic scattering process, we just make the exchange of new couplings $\bar{g}_R \rightleftarrows \bar{g}_L$ in the differential cross section in Eq. (4).

The cross section for the process $\nu_e e \rightarrow \nu_e e$ is obtained by integrating Eq. (4). The experimental cross section for this process is measured in colliders, and due to the neutrino energies, the cross section can be calculated in the approximation $m_e \ll E_\nu$. In that approximation, the cross section is [5,7]

$$\sigma(\varepsilon_{ee}^{eR}, \varepsilon_{ee}^{eL}) \approx \int_0^{E_\nu} dT \frac{d\sigma(E_\nu, T)}{dT} \\ = \frac{2m_e G_{\text{F}}^2 E_\nu}{\pi}\left(\bar{g}_L^2 + \frac{1}{3}\bar{g}_R^2\right). \quad (6)$$

Calculating the antineutrino cross section involves the knowledge of the antineutrino production flux (spectrum), the energy resolution function and, in some cases, other reactor characteristics, for instance, the efficiency. In a previous analysis, the authors of Ref. [6] used a resolution function in the form of a Gaussian distribution with mean T and variance $\sim T'^{0.7}$, only for the MUNU experiment [14]. We reanalyzed the MUNU experiment using the Gaussian resolution, also testing with another variance $\sim T'^{0.57}$ [15], and we did not find a difference compared with our calculus, ignoring the resolution effects. In the last case, the cross section used has the following form:

$$\sigma(\varepsilon_{ee}^{eR}, \varepsilon_{ee}^{eL}) = \int_{T_{\text{min}}}^{T_{\text{max}}} dT \int_{E_{\text{min}}(T)}^{E_{\text{max}}} dE_\nu \lambda(E_\nu)\frac{d\sigma}{dT}(E_\nu, T), \\ \lambda(E_\nu) = \sum_{k=1}^{4} a_k\phi_k(E_\nu), \quad (7)$$

where $\lambda(E_\nu)$ is the spectrum of the fission elements ^{345}U, ^{239}Pu, ^{241}Pu, and ^{238}U, $\phi_k(E_\nu)$ is the flux parametrization and a_k the abundance for each element.

The integration limits in Eq. (7), T_{min} and T_{max}, are the cinematic cuts fixed by the experiments. The energy limit E_{max} is essentially given by the end of the spectrum (~ 9 MeV), and $E_{\text{min}}(T) = 0.5(T + \sqrt{T^2 + 2m_e T})$ [16].

B. Geometrical form of the restriction

Comparing the theoretical cross sections with the experimental ones, and fixing the SM couplings g_P^e (or the value of $\sin^2\theta_W = 0.2326$ including radiative corrections [7]), we obtain the restriction of the NSNI parameters ε_{ee}^{eP}. We used LSND, Irvine, Rovno, and MUNU experiments from the literature [6]. And we added, up to our knowledge, for the first time in this kind of analysis, LAMPF [9], Krasnoyarsk [10], and the latest Texono data [11]. The new experimental results to be used in our analysis are shown in Table I.[1]

---

[1]In fact, these new experiments were used to leptonically determine the Weinberg angle ($\sin^2\theta_W$) [17] or to constrain another NSNI parameter [18].

For the antineutrino case, we used the theoretical flux parametrization from [19], for almost all experiments except for Rovno, in which case we used the parametrization from [20]. We also used the average abundances $a_1 = a_{(^{345}\text{U})} = 54\%$, $a_2 = a_{(^{239}\text{Pu})} = 33\%$, $a_3 = a_{(^{241}\text{Pu})} = 6\%$, and $a_4 = a_{(^{238}\text{U})} = 7\%$ over an annual reactor cycle [14].

In the MUNU case, the available measurement is the event rate. Then, we calculate that rate including a normalization in the theoretical flux N, with the purpose of parametrizing our ignorance on the reactor efficiency $\tilde{\varepsilon}$ ($N^{-1} \sim \tilde{\varepsilon}$).

We define the integrals of the differential cross section in Eq. (7) in the form:

$$\tilde{I}_i = \int_{T_{\min}}^{T_{\max}} dT \int_{E_{\min}(T)}^{E_{\max}} \lambda(E_\nu)\sigma_i(E, T), \qquad (8)$$

where $\sigma_i(E, T)$ is the differential cross section coefficient of the NSNI parameter. Then we find

$$\sigma(\varepsilon_{ee}^{eR}, \varepsilon_{ee}^{eL}) = \tilde{I}_1\bar{g}_R^2 + \tilde{I}_2\bar{g}_L^2 - \tilde{I}_3\bar{g}_R\bar{g}_L. \qquad (9)$$

From Eqs. (6) and (9), we obtain ellipses in the NSNI parameters. The ellipses in the antineutrino case are rotated by an angle $\tan(2\varphi) = \tilde{I}_3/(\tilde{I}_1 - \tilde{I}_2)$, while for neutrino scattering, the ellipses are not, because in the approximation $m_e \ll E_\nu$, the term $\tilde{I}_3$ is negligible.

To quantify the region for each parameter, we use the χ^2 analysis in the way detailed in the next section.

C. The χ^2 analysis

We use the usual definition for the χ^2 function:

$$\chi^2(\varepsilon_{ee}^{eR}, \varepsilon_{ee}^{eL}) \equiv \sum_i \frac{[\sigma_i(\varepsilon_{ee}^{eR}, \varepsilon_{ee}^{eL}) - \sigma_i^{\exp}]^2}{\Delta_i^2}, \qquad (10)$$
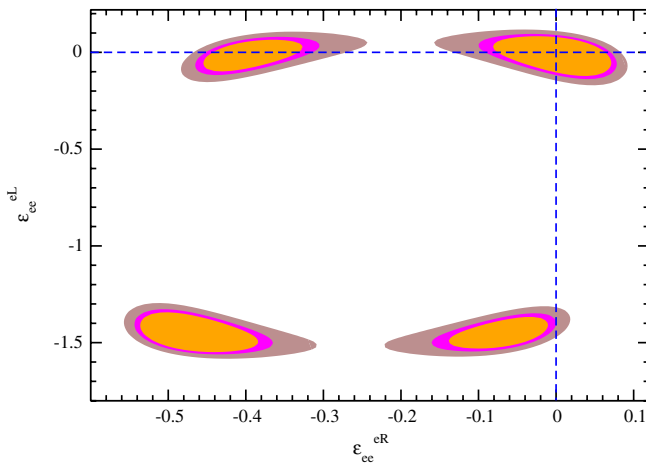

FIG. 1 (color online). Contours at 90% (darker internal part of each region), 95% (90% region plus wrapped region), and 99% (sum of all regions) C.L.

TABLE II. Constraints of the NSNI parameters ε_{ee}^{eP} around the SM point at 90% C.L. related to Fig. 1. See text for further explanation about these constraints.

From Fig. 1	Reference [6]
$-0.08 < \varepsilon_{ee}^{eR} < 0.07$	$-0.07 < \varepsilon_{ee}^{eR} < 0.15$
$-0.12 < \varepsilon_{ee}^{eL} < 0.08$	$-0.13 < \varepsilon_{ee}^{eL} < 0.12$

where $\sigma_i^{\exp}$ and Δ_i are the measurement of the cross section and its error, respectively, for the i experiment. Minimizing Eq. (10) using the theoretical cross section from Eqs. (6) and (9), we obtain the regions of the right panel in Fig. 1.

These four regions are the result of the functional dependence of the cross section of Eq. (6), which are ellipses with horizontal main axes in the NSNI parameter space intercepted by ellipses with vertical main axes derived from the antineutrino cross section given by Eq. (9).

Each region of Fig. 1 is calculated from $\chi^2_{\min} + \Delta\chi^2$. The fixed value for $\Delta\chi^2 = 4.61, 5.99, 9.21$, for two parameters, corresponds to 90%, 95%, and 99% C.L., respectively. We find $\chi^2_{\min} = 6.17$ for 8 experiments so, we have 6 degrees of freedom (d.o.f).

Our regions are smaller than the corresponding one found in Ref. [8], which is significative from the contour at 99% C.L., now defining four separated regions. The SM point (0, 0) is included at 90%.

In Table II, we summarize our constraints for ε_{ee}^{eR} and ε_{ee}^{eL} and compare with previous limits around the SM region using only the scattering data [6]. In the first column, we show the largest range of ε_{ee}^{eR} regardless of the value of remaining parameter ε_{ee}^{eL} and vice-versa. In other words, this analysis allows the remaining parameter to freely varying.

We observe that our parameter constraints are more restricted than those ones presented in Ref. [6], shown in the second column of Table II.

III. PAIR ANNIHILATION IN NEUTRINOS

The first analysis to restrict the NSNI parameters with the process $e^+e^- \to \nu\bar{\nu}\gamma$ was made by the authors of Ref. [5], and later, updated with more experiments in Ref. [8]. We follow both approaches adding even more data.

A. Cross section

Taking into consideration both SM and NSNI interactions, the total cross section can be written as $\sigma = \sigma^{\text{SM}} + \sigma^{\text{NS}}$. In the "radiator" approximation to describe the photon emission, the cross section for the process $e^+e^- \to \nu\bar{\nu}\gamma$ can be calculated as [5]

$$\sigma(s) = \int dx \int dy H(x, y; s)\sigma_0(\hat{s}), \qquad (11)$$

where $x = \frac{2E_\gamma}{\sqrt{s}}$, $\sqrt{s}$ is the center-of-mass energy, $\hat{s} = (1 - x)s$, $y = \cos\theta_\gamma$ (photon angle), σ_0 is the "bare" cross section (without the photon vertex) and $H(x, y; s)$ represents the probability to "radiate" a photon in a scale s, the fraction energy x in the center-of-mass reference.

We use the radiation function $H(x, y; s)$ from [21]

$$H^{(\alpha)}(x, y; s) = \frac{2\alpha}{\pi} \frac{1}{x} \frac{1}{1 - y^2} \left[\left(1 - \frac{x}{2}\right)^2 + \frac{x^2 y^2}{4} \right], \quad (12)$$

where α is the fine structure constant. The bare SM cross section is given by

$$\begin{aligned}
\sigma_0^{SM}(s) = &\frac{N_\nu G_F^2}{6\pi} M_Z^4 ((g_R^e)^2 + (g_L^e)^2) \frac{s}{[(s - M_Z^2)^2 + (M_Z \Gamma_Z)^2]} \\
&+ \frac{G_f^2}{\pi} M_W^2 \left\{ \frac{s + 2M_W^2}{2s} - \frac{M_W^2}{s}\left(\frac{s + M_W^2}{s}\right) \right. \\
&\times \log\left(\frac{s + M_W^2}{M_W^2}\right) - g_L^e \frac{M_Z^2(s - M_Z^2)}{[(s - M_Z^2)^2 + (M_Z \Gamma_Z)^2]} \\
&\times \left. \left[\frac{(s + M_W^2)^2}{s^2} \log\left(\frac{s + M_W^2}{M_W^2}\right) - \frac{M_W^2}{s} - \frac{3}{2} \right] \right\}, \quad (13)
\end{aligned}$$

and the bare NSNI cross section is

$$\begin{aligned}
\sigma_0^{NS}(s) = &\sum_{\alpha = e, \mu, \tau} \frac{G_F^2}{6\pi} s \left[((\varepsilon_{\alpha\alpha}^{eL})^2 + (\varepsilon_{\alpha\alpha}^{eR})^2) \right. \\
&\left. - 2(g_L^e \varepsilon_{\alpha\alpha}^{eL} + g_R^e \varepsilon_{\alpha\alpha}^{eR}) \frac{M_Z^2(s - M_Z^2)}{[(s - M_Z^2)^2 + (M_Z \Gamma_Z)^2]} \right] \\
&+ \frac{G_F^2}{\pi} \varepsilon_{ee}^{eL} M_W^2 \left[\frac{(s + M_W^2)^2}{s^2} \log\left(\frac{s + M_W^2}{M_W^2}\right) \right. \\
&\left. - \frac{M_W^2}{s} - \frac{3}{2} \right], \quad (14)
\end{aligned}$$

where N_ν is the number of active neutrinos, M_W and M_Z are the boson W and Z masses, respectively, and Γ_Z is the total decay rate of Z.

B. Geometrical form of the constraints

The same procedure is used in the scattering, Sec. II B, fixing the SM couplings g_P^e to restrict the NSNI parameters $\varepsilon_{\alpha\alpha}^{eP}$ ($\alpha = e, \tau$) and comparing the cross section from Eq. (11) with the measured cross section. The cross section for the process $e^+ e^- \to \nu\bar{\nu}\gamma$ was measured in the four LEP experiments: ALEPH, DELPHI, OPAL, and L3 [12].

We take the data from Refs. [8,12] and add new data from the DELPHI experiment [13] shown in Table III.

Table III shows the center-of-mass energy $\sqrt{s}$, the cross section σ^{exp} in pico barns, the expected cross section σ^{MC}, the number of events N_{obs}, and the cinematic cuts for the photon energy x and angle y, respectively.

To constrain the NSNI parameters of electronic flavor ε_{ee}^{eP}, we perform the variation of the two parameters at the same time, as we did in the scattering case, defining the others as zero ($\varepsilon_{\tau\tau}^{eP} \equiv 0$). To constrain the tauonic parameters $\varepsilon_{\tau\tau}^{eP}$, we assume $\varepsilon_{ee}^{eP} \equiv 0$.

At this point it is convenient to define

$$I_i \equiv \int dx \int dy H(x, y; s) [\sigma_0^{NS}(\hat{s})]_i, \quad (15)$$

where $[\sigma_0^{NS}(\hat{s})]_i$ refers to the NSNI cross section as a coefficient of the NSNI parameter.

For the electronic flavor parameters ε_{ee}^{eP} from Eq. (11), and using Eq. (15), the geometrical form of the cross section can be written as

$$\sigma^{NS}(\varepsilon_{eR}^{ee}, \varepsilon_{eL}^{ee}) = I_1 [(\varepsilon_{ee}^{eL})^2 + (\varepsilon_{ee}^{eR})^2] + I_2 \varepsilon_{ee}^{eL} + I_3 \varepsilon_{ee}^{eR} \quad (16)$$

then, the cross section is now a circle in the NSNI parameter space.

For the tauonic flavor parameters $\varepsilon_{\tau\tau}^{eP}$, we have the same geometrical form but the coefficient I_2 from Eq. (16) is different, because in that integral the last term of the Eq. (14) is null for tauonic flavor. Using the definition in Eq. (15), the coefficient of $\varepsilon_{\tau\tau}^{eL}$ is

$$\tilde{I}_2 = \frac{g_L^e}{g_R^e} I_3, \quad (17)$$

TABLE III. DELPHI data [13]. Cinematic cuts in the photon energy E_γ are reported like $x = E_\gamma / (E_{beam}) = 2E_\gamma / \sqrt{s}$ and in the photon angle as $y = \cos\theta_\gamma$.

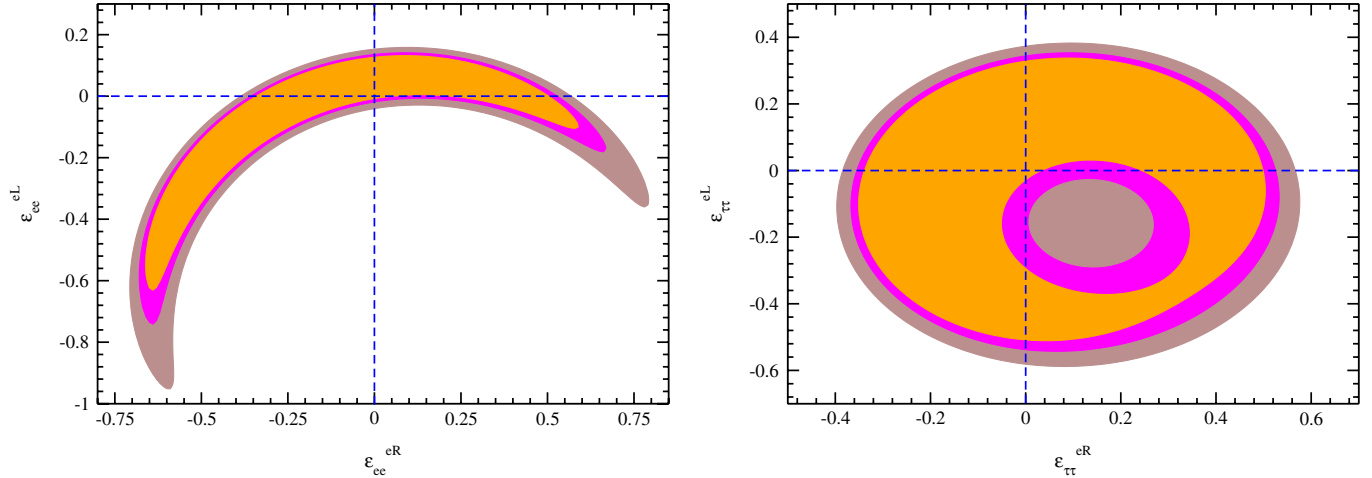| $\sqrt{s}$(GeV)	σ^{exp} (pb)	σ^{MC} (pb)	N_{obs}	E_γ (GeV)	$|y|$
187.1	1.78 ± 0.13	1.89	177	$x \geq 0.06$	≤ 0.71
196.8	1.41 ± 0.13	1.75	127	$x \geq 0.06$	≤ 0.71
205.4	1.50 ± 0.11	1.61	190	$x \geq 0.06$	≤ 0.71
187.1	1.98 ± 0.14	1.97	220	$0.2 \leq x \leq 0.9$	$0.85 \leq |y| \leq 0.98$
196.8	1.71 ± 0.14	1.76	175	$0.2 \leq x \leq 0.9$	$0.85 \leq |y| \leq 0.98$
205.4	1.71 ± 0.12	1.57	224	$0.2 \leq x \leq 0.9$	$0.85 \leq |y| \leq 0.98$
187.1	1.37 ± 0.14	1.44	126	$0.3 \leq x \leq 0.9$	$0.998 \leq |y| \leq 0.990$
196.8	1.22 ± 0.14	1.29	90	$0.3 \leq x \leq 0.9$	$0.998 \leq |y| \leq 0.990$
205.4	1.12 ± 0.11	1.18	114	$0.3 \leq x \leq 0.9$	$0.998 \leq |y| \leq 0.990$

FIG. 2 (color online). Left panel: contours at 90% (darker internal part of each region), 95% (90% region plus wrapped region), and 99% (sum of all regions) of C.L for the ε_{ee}^{eP} parameters, we find $\chi^2_{\min} = 26.04$. Right panel: contours for the $\varepsilon_{\tau\tau}^{eP}$ parameters, we find $\chi^2_{\min} = 25.83$. We use 37 experiments from [8,12] and Table III, then, we have 35 d.o.f.

then, the NS cross section is

$$\sigma^{\rm NS}(\varepsilon_{\tau\tau}^{eR}, \varepsilon_{\tau\tau}^{eL}) = I_1[(\varepsilon_{\tau\tau}^{eL})^2 + (\varepsilon_{\tau\tau}^{eR})^2] + I_3\left(\frac{g_L^e}{g_R^e}\varepsilon_{\tau\tau}^{eL} + \varepsilon_{\tau\tau}^{eR}\right). \tag{18}$$

To quantify the region for each parameter, we continue using the χ^2 analysis including all data from Refs. [8,12] and Table III.

C. The χ^2 analysis

We use the χ^2 function from Eq. (10), but the experimental error includes not only the statistical and systematical errors, but also an additional 10% of theoretical uncertainty in the cross section data [8].

Minimizing the χ^2 function from Eq. (10), with the data from [8,12] and Table III, and the theoretical cross section from Eq. (16), we obtain the contours $\chi^2_{\min} + \Delta\chi^2$ representing 90%, 95%, and 99% C.L. These contours in ε_{ee}^{eP} are shown in the left panel of Fig. 2.

Again, like in Fig. 1, the SM point (0, 0) is included at 90% of C.L in Fig. 2. Then, the SM continues describing the data. The form of the allowed regions shown in this

TABLE IV. Constraints of the FD NSNI parameters ε_{ee}^{eP} and $\varepsilon_{\tau\tau}^{eP}$ at 90% C.L. Our results are found using the same procedure adopted to find the results shown in Table II.

From Fig. 2 (right) and Fig. 3	6-Parameters, Ref. [8]
$-0.11 < \varepsilon_{ee}^{eR} < 0.05$	$-0.03 < \varepsilon_{ee}^{eR} < 0.18$
$-0.02 < \varepsilon_{ee}^{eL} < 0.09$	$-0.14 < \varepsilon_{ee}^{eL} < 0.09$
$-0.35 < \varepsilon_{\tau\tau}^{eR} < 0.50$	$-0.4 < \varepsilon_{\tau\tau}^{eR} < 0.6$
$-0.51 < \varepsilon_{\tau\tau}^{eL} < 0.34$	$-0.6 < \varepsilon_{\tau\tau}^{eL} < 0.4$

figure is the result of the interception of the circles' LEP data only.

Even before the global analysis, observe that LEP experiments constrain $-0.05 \lesssim \varepsilon_{ee}^{eL} \lesssim 0.15$ more than the $-0.35 \lesssim \varepsilon_{ee}^{eR} \lesssim 0.55$ parameter around SM point (0, 0). Because of the form of the constrained region (one region, left panel of Fig. 2) we expect in the global analysis (including the four regions of the scattering data, contours of Fig. 1) the decreasing of the number of regions appearing in Fig. 1.

The authors of Ref. [5] were the first to notice the importance of the process $e^+e^- \to \nu\bar{\nu}\gamma$ to constrain the $\varepsilon_{\tau\tau}^{eP}$ parameters, due to the lack of cross section data for τ elastic scattering. To constrain those parameters we use a χ^2 function analog as Eq. (10):

$$\chi^2(\varepsilon_{\tau\tau}^{eR}, \varepsilon_{\tau\tau}^{eL}) \equiv \sum_i \frac{[\sigma_i(\varepsilon_{\tau\tau}^{eR}, \varepsilon_{\tau\tau}^{eL}) - \sigma_i^{\exp}]^2}{\Delta_i^2}, \tag{19}$$

where $\sigma_i(\varepsilon_{\tau\tau}^{eR}, \varepsilon_{\tau\tau}^{eL})$ is given by Eq. (18).

In the right panel of Fig. 2 are shown the contours for these parameters, and the greatest constraints we obtain are $-0.35 < \varepsilon_{\tau\tau}^{eR} < 0.50$ and $-0.51 < \varepsilon_{\tau\tau}^{eL} < 0.34$ at 90% C.L. All the constraints on $\varepsilon_{\tau\tau}^{eP}$ are summarized in Table IV. Note that here we use the same procedure previously used to find Table II (see corresponding explanation in the text). Also shown in this Table are the results of the six parameter variation realized in Ref. [8]. Note that our results are systematically more restrictive.

IV. GLOBAL ANALYSIS

Putting together the two main χ^2 statistics we have made, from neutrino elastic scattering $\chi^2_{\rm elast}$ and pair
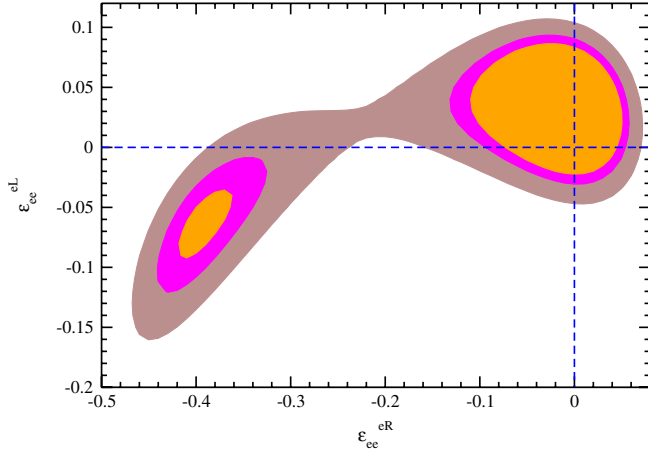
FIG. 3 (color online). Contours at 90% (darker internal part of each region), 95% (90% region plus wrapped region), and 99% (sum of all regions) C.L. for the ε_{ee}^{eP} parameters, using scattering and par annihilation data (global analysis). We find $\chi^2_{\text{glob}_{\min}} = 34.31$ using 45 experiments, then we have 43 d.o.f.

annihilation process χ^2_{lep}, we calculated the constraints on the ε_{ee}^{eP} allowed for terrestrial experiments.

From the minimization of $\chi^2_{\text{glob}} = \chi^2_{\text{elast}} + \chi^2_{\text{lep}}$ function, we obtain the Fig. 3. As in Figs. 1 and 2, the SM point (0, 0) is included at 90% C.L. in Fig. 3. As we have asserted, the inclusion of the LEP data diminished the number of regions from four to two (see Fig. 3), which is different from what is obtained in Ref. [8]. At 90% and 95% C.L., we also obtain, in the projection around the SM point, one region for each parameter. The existence of a unique global region, even at 99% C.L. depends on the number of parameters which are varying (two or six).

Although the number of regions is different, doing the variation of two parameters at the same time, our constraints are similar but a little more restricted than in Ref. [8], as we show in Table IV.

V. CONCLUSIONS

We use the elastic and pair annihilation processes to constrain the NSNI with electrons calculated from cross sections. From the χ^2 statistics, using only the scattering data, we find four separated allowed regions even at 99% C.L. as we show in Fig. 1. This number of allowed regions is the result of the functional dependence of the cross section, which is an ellipse in the NSNI parameter space. Adding antineutrino data, we find ellipses which are perpendicular to the neutrino ones, producing the four mentioned regions.

From the pair annihilation cross section analysis, we obtain different regions than the one obtained by different authors. We can visualize that, from the LEP circles, the allowed region has to be qualitatively coincident with the one obtained by our χ^2 analysis. Also, we are not surprised with the regions we obtain since they include the SM predictions. The difference between the regions for electronic and tauonic flavor are due to the numerical value for the coefficient I_2.

In Refs. [5,6] the χ^2 analysis was done assuming a variation of one and two parameters simultaneously, and in Ref. [8] a six parameter variation was done. It is not clear which sort of variation is more convenient. In fact, only if one assumes a specific SM extension, this kind of question can be appropriately answered.

In our model independent approach, we perform a two parameter variation and our results are more restrictive than what is obtained for a six parameter variation.

[1] M. C. Gonzalez-Garcia and M. Maltoni, Phys. Rep. **460**, 1 (2008); M. C. Gonzalez-Garcia, M. Maltoni, and J. Salvado, J. High Energy Phys. 04 (2010) 056.
[2] J. L. Rosner, Am. J. Phys. **71**, 302 (2003).
[3] S. Bergmann, Y. Grossman, and D. M. Pierce, Phys. Rev. D **61**, 053005 (2000).
[4] M. B. Gavela, D. Hernandez, T. Ota, and W. Winter, Phys. Rev. D **79**, 013007 (2009).
[5] Z. Berezhiani and A. Rossi, Phys. Lett. B **535**, 207 (2002).
[6] J. Barranco, O. Miranda, C. Moura, and J. Valle, Phys. Rev. D **73**, 113001 (2006).
[7] S. Davidson, C. Pena-Garay, N. Rius, and A. Santamaria, J. High Energy Phys. 03 (2003) 011.
[8] J. Barranco, O. G. Miranda, C. A. Moura, and J. W. Valle, Phys. Rev. D **77**, 093014 (2008).
[9] R. Allen et al., Phys. Rev. D **47**, 11 (1993).
[10] G. S. Vidyakin et al., JETP Lett. **55**, 206 (1992).
[11] M. Deniz et al., Phys. Rev. D **81**, 072001 (2010).
[12] M. Hirsch, E. Nardi, and D. Restrepo, Phys. Rev. D **67**, 033005 (2003).
[13] J. Abdallah et al., Eur. Phys. J. C **38**, 395 (2005)..
[14] Z. Daraktchieva et al., Phys. Lett. B **564**, 190 (2003).

[15] Z. Daraktchieva *et al.* (MUNU Collaboration), Phys. Lett. B **615**, 153 (2005).

[16] P. Vogel and J. Engel, Phys. Rev. D **39**, 3378 (1989).

[17] J. Barranco, O. G. Miranda, and T. Rashba, Phys. Lett. B **662**, 431 (2008).

[18] J. Barranco, O. G. Miranda, and T. Rashba, Nucl. Phys. **B188**, 214 (2009).

[19] P. Huber and T. Schwetz, Phys. Rev. D **70**, 053011 (2004).

[20] F. T. Avignone-III, Phys. Rev. D **2**, 2609 (1970).

[21] O. Nicrosini and L. Trentadue, Nucl. Phys. **B318**, 1 (1989).